Impact of Slot Width on Performance of Symmetrical-Slot-Antenna Resonant-Tunneling-Diode Oscillators

Dinh Tuan Nguyen, Gabriele Picco, Petr Ourednik, Christian Spudat, and Michael Feiginov

***Abstract*—In this article, we show that the output power of symmetrical-slot-antenna resonant-tunneling-diode (RTD) oscillators depends on the slot width. The dependence could be used as a fine-tuning degree of freedom to increase the output power of the oscillators. The fine-tuning mechanism is related to maximizing the RTD-oscillation amplitude by a proper balance between the slot-antenna radiation and ohmic losses, and the slot susceptance. The presented simulation results are in agreement with the experimental data in the frequency range of 150–400 GHz. We report the output powers of 283 μW at 184 GHz and 82 μW at 368 GHz, which are very close to the state-of-the-art literature data for the given type of RTD oscillators.**

***Index Terms*—Oscillators, output power, resonant-tunneling diodes (RTDs), slot antenna, THz sources.**

I. Introduction

THz frequency range is expected to be important for many applications [1], but the lack of sufficiently-simple solid-state room-temperature radiation sources hinders its practical use. Among available technologies, resonant-tunneling-diode (RTD) oscillators stand out as one of the most promising for practical use since sub-THz and THz RTD oscillators are very simple [2], [3], compact [4], they work at room temperature, cover the frequencies up to almost 2 THz [5], [6], can provide relatively high output power radiated into free space (several hundred μW by stand-alone oscillators and up to $\approx$ 10 mW at 0.45 THz in coherent-array configuration) [7], [8], [9], [10], have high DC-to-RF conversion efficiency of up to 1%–5% [7], [9], [11], etc. A number of potential applications were also demonstrated with RTDs: wireless communication [12], [13], imaging [14], spectrometer [15], radars [16], [17], etc. We have to mention that transistor technology is a strong competitor to RTD oscillators (see [18]). The performance of both technologies could be comparable at sub-THz frequencies, although transistor oscillators radiate at higher harmonics in many instances. Fundamental-frequency transistor oscillators operate only at frequencies significantly below 1 THz so far.

Although different types (slot- and patch-antenna, composite, membrane, waveguide-based, etc.) [2], [3], [4], [8], [9], [19], [20], [21] of RTD oscillators were developed, the state-of-the-art performance with regard to high operating frequencies and high output power (from a single oscillator) has been achieved with slot-antenna RTD oscillators so far [5], [6], [7]; even better performance in the terms of the output power was demonstrated with double-RTD oscillator configurations (which could also be deemed as single oscillators) and with coherent arrays [8], [9], [10]. On-chip slot-antenna RTD oscillators are also the simplest and most studied type of RTD oscillators [2], [3]. Two basic variants of such oscillators exist: with symmetric and asymmetric slots [2], [7]. A higher output power can be achieved with the latter ones, although they have a tilted radiation pattern [7], [10], complicating their practical use. The former ones exhibit lower output power, but their radiation pattern is symmetrical (due to the symmetry of the structure), which simplifies coupling of such oscillators with the Gaussian optics of free-space THz systems, dielectric waveguides, and that is also of advantage for power combining in array configurations of oscillators [10], [22]. Therefore, our focus in this work is on symmetrical slot-antenna RTD oscillators.

The radiation of a simple on-chip slot-antenna oscillator is predominantly emitted into the substrate (InP). Such oscillators need to be mounted on a Si lens to outcouple their radiation into free space. The Si lens makes these oscillators relatively bulky. In this respect, other types of oscillators (e.g., patch-antenna RTD oscillators) are more compact since they emit radiation directly into free space upwards, from the ground plane of the chip. In terms of their output power, both the slot- and patch-antenna oscillators perform, in principle, similarly [11].

A symmetrical slot antenna with an RTD in the slot center (both arms of the slot have equal length and width) is defined by two parameters: slot length (l) and width (w). The slot length is chosen according to the target oscillator frequency: the higher the frequency, the shorter the slot. On the other hand, the slot width is typically chosen to be equal to 4 μm in the sub-THz and THz RTD oscillators [5], [11], [23], [24], [25], [26]. Usually, the

Manuscript received 15 June 2023; revised 2 September 2023; accepted 26 October 2023. Date of publication 2 November 2023; date of current version 5 January 2024. This work was supported in part by the Austrian Science Fund (FWF) under Grant P30892-N30 and in part by the TU Wien Bibliothek funded by Open Access Funding Program. *(Dinh Tuan Nguyen, Gabriele Picco, and Petr Ourednik contributed equally to this work.) (Corresponding author: Michael Feiginov.)*

The authors are with the Department of Electrical Engineering and Technology, TU Wien, 1040 Vienna, Austria (e-mail: dinh.nguyen@tuwien.ac.at; gabriele.picco@tuwien.ac.at; petr.ourednik@tuwien.ac.at; christian.spudat@chello.at; michael.feiginov@tuwien.ac.at).

Color versions of one or more figures in this article are available at https://doi.org/10.1109/TTHZ.2023.3329460.

Digital Object Identifier 10.1109/TTHZ.2023.3329460

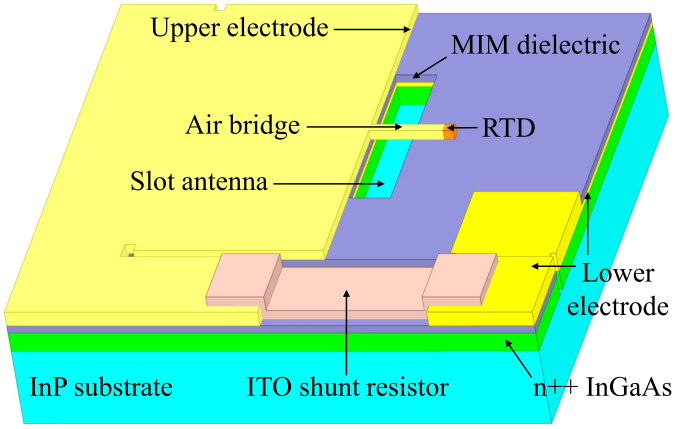

Fig. 1. Schematic of a slot-antenna RTD oscillator.

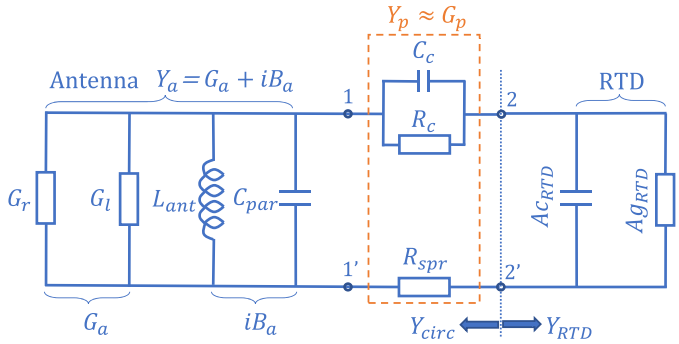

Fig. 2. AC equivalent circuit of an RTD oscillator.

slot width is not used as a degree of freedom in the optimization of the oscillators. There is just one publication [27] where the impact of the variation of the slot width on the characteristics of on-chip symmetrical-slot-antenna RTD oscillators was studied; it should be noted that the impact of the radiator width on the performance of asymmetrical-slot RTD oscillators (where RTD is shifted toward one end of the slot) was studied in more details (see [28]). In [27], it was indicated that the oscillation frequency increases with the decrease in the slot width. This tendency was confirmed by experimental data with 2 and 4 μm wide slot antennas at $\approx$350 GHz. In the same work, it was expected that the output power of RTD oscillators should be almost independent of the slot width.

In this work, we show that the output power of symmetrical-slot-antenna RTD oscillators depends on the slot width. Although the dependence is not very strong for wider slots, it is essential for fine tuning the oscillator performance. Essentially, the mechanism of the influence of the slot width on the oscillator performance is related to maximizing the amplitude of the AC voltage swing on the RTD by finding an intricate balance between the slot ohmic and radiation losses, slot inductance, and RTD area. In this work, we present a detailed analysis of the impact of the slot width on the oscillator characteristics along with experimental data, which are in a good agreement with the theory.

II. Design of Slot-Antenna RTD Oscillators and Their Output Power

A schematic of a slot-antenna RTD oscillator we investigate in this article is shown in Fig. 1. It is a rather common design of RTD oscillators in the sub-THz frequency range [23]. The slot antenna is formed by a rectangular hole in the lower electrode metallization layer and by removing the conducting doped semiconductor layers in the hole. An RTD is positioned on one side of the slot, and an air bridge connects it to the upper electrode of a large metal-insulator-metal (MIM) capacitor on the other side of the slot. The upper and lower electrodes form two contacts to the RTD to supply its DC bias. In addition, a shunt resistor [e.g., made of indium-tin-oxide (ITO)] is fabricated between the upper and lower electrodes parallel to the RTD to suppress parasitic RTD oscillations at low frequencies.

An AC equivalent circuit of an RTD oscillator could be represented in the form shown in Fig. 2. $Y_{\rm a}$ stands for the admittance of the oscillator antenna/resonator (slot antenna in our case) with the susceptance $B_{\rm a}$ and conductance $G_{\rm a}$. The latter has two contributions $G_{\rm a} = G_{\rm l} + G_{\rm r}$, where $G_{\rm r}$ is the antenna radiation conductance, and $G_{\rm l}$ represents the ohmic antenna losses. The RTD admittance also has both real ($A\,g_{\rm RTD}$) and imaginary ($\omega\,A\,c_{\rm RTD}$) parts, where ω is the angular frequency, A is the RTD-mesa area, $g_{\rm RTD}$ and $c_{\rm RTD}$ are the specific (per unit area) RTD conductance and capacitance, respectively. That is a general RTD-admittance model, since $g_{\rm RTD}$ and $c_{\rm RTD}$ are frequency dependent [29], [30], [31], [32]. The model can also take into account the nonlinearity of the RTD characteristics by considering the dependence of $g_{\rm RTD}$ and $c_{\rm RTD}$ on the AC amplitude ($V_{\rm AC}$) [33]. We represent a time-dependent RTD bias ($V(t)$) as a DC bias ($V_{\rm DC}$) with a sinusoidal AC voltage

$$V(t) = V_{\rm DC} + V_{\rm AC}\cos(\omega t). \tag{1}$$

To simplify further analysis and discussion, and since the generation of higher harmonics usually has little influence on the oscillation characteristics of the fundamental RTD oscillators (the higher harmonics are effectively short-circuited by the RTD capacitance), we limit ourselves to the first-harmonic-zone analysis and understand under $g_{\rm RTD} \approx g^{(1)}(\omega, V_{\rm AC}, V_{\rm DC})$ the ratio of the amplitude of the first-harmonic current RTD response to $V_{\rm AC}$. Also, for simplicity, we assume in the further analysis that in the negative-differential-conductance (NDC) region of the RTD I–V curve, the RTD capacitance ($c_{\rm RTD}$) is a constant independent of ω, $V_{\rm AC}$, and $V_{\rm DC}$. The other elements in the circuit in Fig. 2 represent RTD parasitics: RTD contact resistance ($R_{\rm c}$) and capacitance ($C_{\rm c}$), parasitic RTD stray capacitance ($C_{\rm par}$), and the RTD spreading resistance ($R_{\rm spr}$). We include the contribution of $C_{\rm par}$ as a part of antenna susceptance ($B_{\rm a}$). At sub-THz frequencies, the RTD-contact capacitive reactance is negligible compared to its resistance, therefore, we describe the RTD parasitics as real-valued parasitic conductance ($G_{\rm p}$).

In the steady-state oscillation regime, the subsequent equations have to be satisfied at the fundamental oscillation frequency (see notations in Fig. 2)

$$\mathrm{Im}(Y_{\rm circ}) = -A\,\omega\,c_{\rm RTD} \tag{2}$$

$$\mathrm{Re}(Y_{\mathrm{circ}}) = -A\, g^{(1)}(V_{\mathrm{AC}}). \tag{3}$$

Equation (2) defines the fundamental oscillation frequency and (3) determines the steady-oscillation amplitude (V_{AC}). Once (2) and (3) are solved, and a steady-oscillation amplitude V_{AC} is found, the output power (P) of an RTD oscillator can be calculated with the equation [23]

$$P = \frac{1}{2}\left|\frac{Y_{\mathrm{circ}}}{Y_{\mathrm{a}}}\right|^2 G_{\mathrm{r}} V_{\mathrm{AC}}^2. \tag{4}$$

III. Simplified Analysis

We discuss a simplified oscillator model to elucidate the interdependencies between different parameters of the slot-antenna RTD oscillators and the mechanism of how the slot width affects the output power. The model is based on two essential simplifications: (i) we neglect the RTD contact and stray parasitics (G_{p} and C_{par}) in the equivalent model in Fig. 2; (ii) we use a narrow-slot approximation, i.e., we assume that the slot-antenna radiation conductance and antenna loss resistance are independent of the slot width and determined only by the slot length; we also neglect the air-bridge inductance compared to that of the slot antenna. At the lower side of the sub-THz frequency range, those are often accurate approximations [11]; in the middle of the sub-THz frequency range, these approximations have a semiquantitative character; at THz frequencies, the model is useful for a qualitative discussion, since parasitics become important, and the slot usually becomes quite short, i.e., it cannot be seen as a narrow one anymore.

First, we apply the simplification (i). When G_{p} is neglected, the factor $|Y_{\mathrm{circ}}/Y_{\mathrm{a}}|$ is equal to 1, and it disappears in (4). Then, the output power of an RTD oscillator (4) can be represented [11] as

$$P = \frac{1}{2} G_{\mathrm{r}}\, \Delta V^2\, (1-\gamma)\, \alpha(\gamma) \tag{5}$$

where we substituted $V_{\mathrm{AC}}^2 = \Delta V^2(1-\gamma)\alpha(\gamma)$ and defined

$$\gamma = \frac{g^{(1)}}{g_0} = -\frac{G_{\mathrm{r}} + G_{\mathrm{l}}}{g_0\, A}. \tag{6}$$

g_0 is the maximum of the differential RTD NDC ($g_0 < 0$), ΔV is the voltage separation between the peak and valley points of the RTD I–V curve. In the regime of the onset of oscillations, when V_{AC} is very small, (3) should be replaced by an inequality $\mathrm{Re}(Y_{\mathrm{circ}}) < -A\, g_0$, and V_{AC} is growing with time. $|g^{(1)}|$ is decreasing with the growth of V_{AC} and the growth of V_{AC} stops when (3) is satisfied, i.e., $A|g^{(1)}|$ is exactly equal (in the framework of the first-harmonic-zone analysis) to the antenna/circuit losses in the stationary-oscillation regime. The parameter γ defined by (6) describes how much the RTD NDC is reduced in the steady-oscillation regime compared to its differential (maximum) value g_0; in such a way, the parameter γ is related to the oscillation amplitude V_{AC}. The second identity in (6) follows from (3) if one neglects G_{p}. For a third-order polynomial approximation of the RTD I–V curve, $|g^{(1)}|$ is a monotonously decreasing function of V_{AC}. Correspondingly, $\gamma \to 1$ when $V_{\mathrm{AC}} \to 0$ and $\gamma \to 0$ at the maximum of V_{AC} (where $g^{(1)}$ is still negative). For an RTD I–V curve approximated by a third-order polynomial, the coefficient α is equal to 1, and it can be disregarded. In the general case (for a real I–V curve that cannot be approximated by a third-order polynomial), $g^{(1)}$ could be a nonmonotonous function of V_{AC} for a given V_{DC}. However, one can define an envelope function describing a maximal (negative) $g^{(1)}(V_{\mathrm{AC}})$ achievable for a given V_{AC} at different V_{DC} [11]. This envelope function recovers a monotonous dependence on V_{AC} and, in the following, we will understand this envelope function under $g^{(1)}(V_{\mathrm{AC}})$ in (6) for real RTD I–V curves. The parameter $\alpha(\gamma)$ is then a correction coefficient for the output power of an RTD oscillator for a real RTD I–V curve. For a typical RTD I–V curve, $\alpha(\gamma)$ is decreasing monotonously with the increase of γ from $\alpha \approx 2$ at $\gamma \approx 0$ to $\alpha \ll 1$, when $\gamma \to 1$ (see details in [11]).

Equation (5) indicates two considerations important for optimization of the parameters of RTD oscillators to increase their output power. On the one hand, one can increase the output power by increasing G_{r}, if the slot antenna is made longer and operates closer to its eigenfrequency. On the other hand, one should reduce the parameter γ: essentially, that leads to the increase of the AC amplitude (V_{AC}). However, these two approaches are not quite compatible: operating the slot antenna close to its eigenfrequency will require a small RTD-mesa area (A) and, according to (6), will increase γ. Therefore, there is a certain optimum in the choice of the slot-antenna parameters and RTD area. Here, we give qualitative considerations on how to adjust the slot-antenna parameters to increase the oscillator output power.

In the beginning, we exclude A from (6). In the framework of the simplified model, where G_{p} is neglected, one gets from (2)

$$A = -\frac{B_{\mathrm{a}}}{\omega\, c_{\mathrm{RTD}}}. \tag{7}$$

Then, we can rewrite the second identity in (6) as

$$\gamma = \omega \tau_{\mathrm{RTD}} \frac{G_{\mathrm{r}} + G_{\mathrm{l}}}{B_{\mathrm{a}}} \tag{8}$$

where τ_{RTD} is the RTD RC time constant equal to c_{RTD}/g_0. τ_{RTD} has a fixed value for a given RTD wafer, defined by the epitaxial RTD layers.

As a next step, we fix the frequency ω and the slot-antenna length (l) and try to adjust the other parameters of a slot-antenna RTD oscillator to maximize its output power (5). By fixing l, we assume the radiation conductance (G_{r}) of the antenna to be also fixed since G_{r} of a narrow slot antenna is predominantly determined by its length and its dependence on the slot width (w) is weak [34]. Then, the oscillator output power, see (5), could be influenced and increased only by minimizing the parameter γ. According to (8), γ can be influenced only by the variations of G_{l} and B_{a} with the variation of the slot width w since G_{r} is fixed for given l. We note that the total slot-antenna conductance $G_{\mathrm{a}} = G_{\mathrm{r}} + G_{\mathrm{l}}$ is usually small compared to the antenna susceptance $|B_{\mathrm{a}}|$. In this case, we can express the antenna parallel (see Fig. 2) loss conductance as $G_{\mathrm{l}} \approx R_{\mathrm{l}} B_{\mathrm{a}}^2$ via the loss resistance R_{l}, connected in series with B_{a} and G_{r}. This transformation is helpful since the slot-antenna ohmic losses originate from the antenna-surface currents flowing around the circumference

of the antenna. For a narrow slot, the antenna circumference is nearly constant for a fixed l. Therefore, R_l is also nearly constant in this case; it is predominantly determined by the antenna length (for a fixed ω). Then, the only free parameter in the definition of γ influenced by the slot width is B_a, and we can rewrite (8) as

$$\gamma = \omega\tau_\mathrm{RTD}\left(\frac{G_\mathrm{r}}{B_\mathrm{a}} + R_\mathrm{l}B_\mathrm{a}\right). \tag{9}$$

Equation (9) has a minimum and P in (5) a maximum, when

$$B_\mathrm{a} = -\sqrt{\frac{G_\mathrm{r}}{R_\mathrm{l}}}. \tag{10}$$

This condition corresponds to the equation

$$G_\mathrm{r} = G_\mathrm{l} \tag{11}$$

i.e., if the antenna losses are dominated by the radiation (G_r), then we can reduce γ by increasing B_a, see (9); on the other hand, if the antenna losses are dominated by the ohmic losses (G_l), then we can reduce γ by reducing B_a; γ is minimized when the radiation and ohmic losses of a slot antenna are equal (in the framework of the described simple model).

For a short slot antenna, when its length is small compared to the wavelength, i.e., the antenna is operated significantly below its eigenfrequency, the slot antenna behaves as an inductance (L), and B_a could be expressed as $B_\mathrm{a} = -1/\omega L$ (we disregard C_par in the simplified model). Qualitatively, one can think of the slot antenna in this regime as a current loop around a slot-shaped hole in a metal plane. When the slot length is fixed, the area of the loop (and its inductance L) is determined by the slot width. The larger the width w, the larger the inductance L and the smaller $|B_\mathrm{a}|$. In such a way, we can adjust B_a by changing the slot width to take an optimum value given by (10) or (11). For each slot length l, there should exist an optimum value of the slot width w. The required RTD-mesa area for the chosen slot parameters is defined by (7).

It is important to notice, the relations (10) and (11) determining an optimum slot width are independent of RTD parameters. Essentially, these are universal relations for a slot antenna in an RTD oscillator; they define an optimum slot geometry, i.e., for every slot length (l), (10) and (11) define a matching optimum slot width (w) to minimize γ and to give a "conditional" maximum to P (for a fixed l). However, an optimum slot geometry is different for different frequencies since G_r and G_l (or R_l) are dependent on frequency. R_l (or G_l) and an optimum slot geometry are also dependent on the material slot composition since R_l originates from the skin-effect ohmic losses.

On the other hand, an optimum slot length for a given frequency is RTD specific since τ_RTD in γ in (8) and $\alpha(\gamma)$ in (5) are RTD parameters. Thus, to find an optimum l, one needs to find a maximum of (5). However, in the framework of the simplified model above, one can find an optimum l and the maximum output power rather easily. To this end, we substitute G_l and (10) and (11) for the optimized B_a into (8) and get the following expression for the optimum γ:

$$\gamma = -2\omega\tau_\mathrm{RTD}\sqrt{G_\mathrm{r}R_\mathrm{l}}. \tag{12}$$

Note, G_r and R_l are functions solely of l in this model, specifically, $G_\mathrm{r} \propto l^2$ and $R_\mathrm{l} \propto l$. Having defined an optimum γ for each l with (12), we substitute it into (5) and can calculate the output power at a given frequency as a function of l. This dependence goes to zero at $l \to 0$, since G_r in (5) goes to zero in this limit. On the other hand, (5) goes to zero when $\gamma \to 1$. In between, there is a ("global") maximum of the oscillator output power at a certain value of l, which defines an optimum slot length.

In the foregoing analysis, we relied on certain simplifying assumptions concerning the dependence of the slot-antenna admittance on the slot geometry. To justify these assumptions, we provide approximate analytic equations for G_r and B_a of a slot antenna, which are derived using the Babinet principle and approximate equations for a small (Hertz) dipole [34]

$$G_\mathrm{r} = \frac{2\pi}{3Z_\mathrm{eff}}\left(\frac{l}{\lambda_\mathrm{eff}}\right)^2 \tag{13}$$

$$B_\mathrm{a} = -\frac{4}{\pi Z_\mathrm{eff}}\frac{\ln(l/w) - 1}{\tan(\pi l/\lambda_\mathrm{eff})} \tag{14}$$

where $Z_\mathrm{eff} = Z_0/\sqrt{\varepsilon_\mathrm{eff}}$ is an effective impedance, Z_0 is the free-space impedance, $\varepsilon_\mathrm{eff} = (\varepsilon_\mathrm{s} + 1)/2$ is an effective dielectric constant at the interface between the air and substrate (InP in our case, with the dielectric constant ε_s), $\lambda_\mathrm{eff} = \lambda_0/\sqrt{\varepsilon_\mathrm{eff}}$ is an effective wavelength, λ_0 is the radiation wavelength in free space. Equations (13) and (14) are asymptotically valid for small ($\lambda_\mathrm{eff} \ll l$) slots formed by an infinitely-thin ideally conducting metal layer on a dielectric substrate. These equations support the asymptotic relations and simplifications, we used in the foregoing analysis (although we did not use these equations explicitly in our analysis): $G_\mathrm{r} \propto l^2$, and G_r is independent of w; B_a is only weakly (logarithmically) changing with w.

IV. Numerical Simulations

The foregoing discussion is semiquantitative in nature. It relies on several simplifying assumptions, as described above. To give an accurate picture and to compare it with the simplified model above, we present numerical simulation results for the dependence of the output power on the geometrical slot parameters. As a first step, we keep the RTD contact parasitics neglected but use accurate simulation data for the antenna characteristics, i.e., we keep the simplifying assumption (i) and relax the second one (ii). As a second step, we also include RTD contact parasitics in the numerical simulations, i.e., relax the assumption (i) as well.

To be specific, we make the simulations for an RTD wafer with the layer parameters shown in Fig. 3. This RTD wafer has 1.6 nm AlAs barriers and exhibits the peak current density of 5.8 mA/μm^2 with a peak-to-valley current ratio of 9 (see Fig. 4). Those are typical parameters for RTDs used in the sub-THz frequency range. In the past, we have used this wafer in the RTD oscillators, working at frequencies of $\approx$ 100–500 GHz [11], [35]. We also use this RTD wafer in the experimental part of this work.

For the simulation of the antenna characteristics (admittance, radiation, and loss conductances, etc.), we used a commercial electromagnetic simulator (ANSYS HFSS). For given slot-antenna dimensions, the simulated antenna admittance is substituted into (2) and (3), the equations are then solved for different

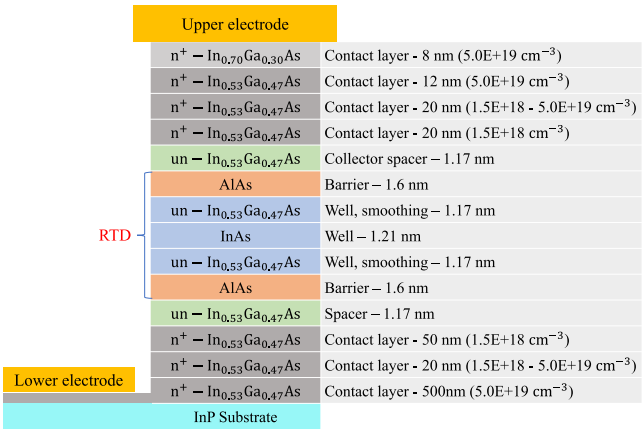

Fig. 3. RTD-wafer parameters.

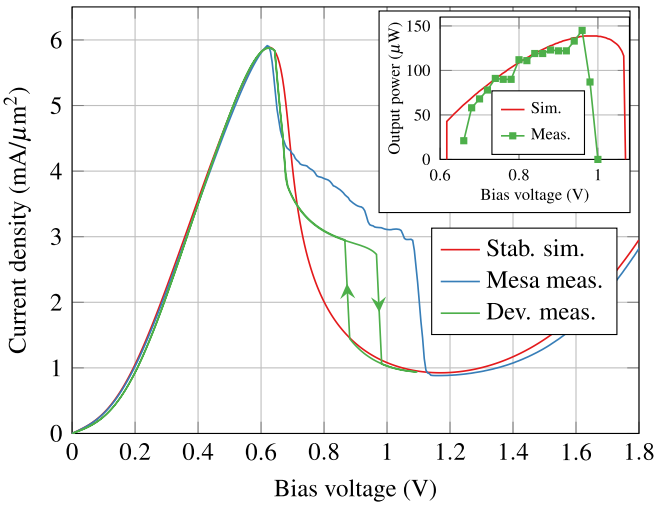

Fig. 4. I–V curves of a 2.0 μm^2 RTD integrated with a slot antenna with 150 μm length. The measured I–V curve is shown in green, the simulated one in red, and the I–V curve of a free-standing RTD is shown in blue. The inset shows the dependence of the oscillator output power on the bias voltage.

RTD areas (A), giving the corresponding oscillation frequencies and the steady-oscillation amplitude (V_{AC}). Afterward, in the general case, the oscillator output power is calculated with (4).

In the case when the RTD parasitics are neglected, the simulation procedure becomes more simple. $\mathrm{Im}(Y_{\mathrm{circ}})$ in (2) becomes equal to B_{a}. Substituted into (2), it defines the oscillation frequency, or (7) defines the RTD area A for an oscillator working at a given frequency. For calculation of the output power, one can use then directly (5) and (6). Example simulation results are shown in Fig. 5.

Fig. 5 shows that without the contribution of the RTD contact parasitics, the slot-antenna RTD oscillators at 375 GHz should achieve the maximum output power of around 138 μW for the given RTD wafer when the slot width is 4–5 μm and the slot length is 80–90 μm. The figure shows a clear global maximum for certain values of the slot width and length, in accord with the qualitative explanations in the previous chapter: there is a "conditional" maximum of the output power at a certain slot

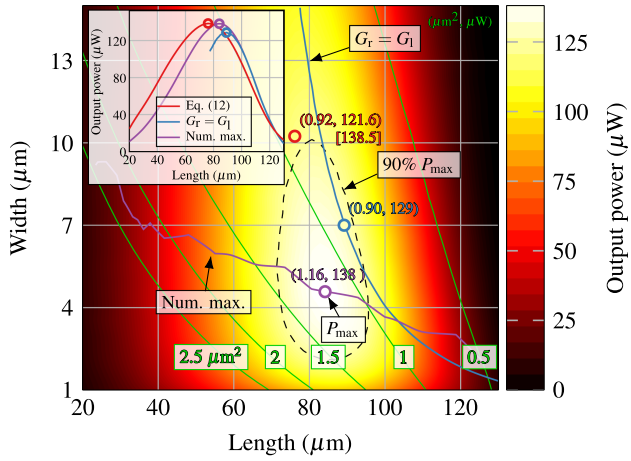

Fig. 5. Map of the output power for different slot-antenna length and width for an RTD oscillator operating at 375 GHz, RTD parasitics are neglected. The blue line shows the optimal dimensions from the condition $G_{\mathrm{r}} = G_{\mathrm{l}}$, the purple line corresponds to maxima along w axis according to the numerical simulations. The green contour lines show the required RTD area in μm^2. The dashed black contour line shows 10% deviation from the maximum output power of the plot. The inset shows the maximum powers resulting from the condition $G_{\mathrm{r}} = G_{\mathrm{l}}$ (blue), the numerical maxima (purple), and (12) (red) for G_{r} and R_{l} calculated for the slot width of 1 μm. The points in both figures show the maximum power for the corresponding conditions. The values in the round brackets give the corresponding RTD area and the output power according to numerical simulations, respectively; the value in the square brackets corresponds to the maximum (red point) in the inset.

width for every slot length; then, when we change l and follow the "conditional" maxima, we find a "global" maximum at a certain antenna length.

In Fig. 5, we show with a purple line the positions of the "conditional" output-power maxima along w axis for each slot length. For a comparison, we also show a blue line with $G_{\mathrm{r}} = G_{\mathrm{l}}$ in Fig. 5, where the output power should get maximum with the variation of w, according to (11) in the framework of the simplified analysis. The curves are somewhat deviating from each other (due to a weak dependence of the slot-antenna characteristics on w for shorter antennas). Nevertheless, the blue curve passes very close to the global output-power maximum. An inset in Fig. 5 shows the variation of the oscillator output power along the purple and blue lines with the variation of the slot length. Both maxima are quite close to each other. The maximum along the blue line is at ≈ 129 μW, when the slot length is ≈ 90 μm, and the slot width is ≈ 7 μm, which is indeed quite close to the global maximum. For a comparison, we also plot in the inset of Fig. 5, the output power calculated with (12) substituted into (5), where G_{r} and R_{l} are calculated for a narrow slot with a width of 1 μm. This maximum is at ≈ 138.5 μW, when the slot length is ≈ 75 μm and the slot width is ≈ 10 μm, the latter corresponds to B_{a} given by (10). This slot width might look somewhat far off the global maximum. Yet, it is within the yellow region in Fig. 5, i.e., within the parameter space of the slot dimensions just $\approx 10\%$–15% below the global output power maximum, which is a reasonably-good range of the parameter space. The deviations of the approximate curves (red and blue) from the accurate one (purple) are because G_{r} and G_{l} were considered independent of w in the simplified analysis.

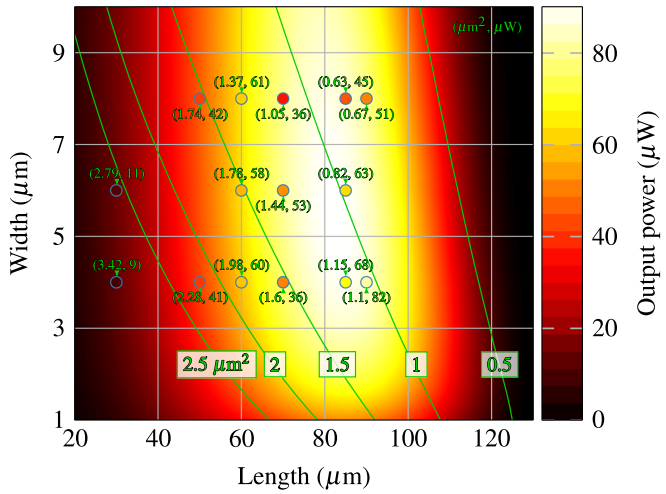

Fig. 6. Color map of the output power of slot-antenna RTD oscillators at 375 GHz. The green contour lines show the design RTD-mesa area in μm^2 to achieve the target oscillation frequency. The color dots represent the experimental data for RTD oscillators working in the frequency range of 375 $\pm$ 10 GHz. The first number next to each dot shows the RTD-mesa area, and the second one gives the output power (also indicated by the dot color) for each oscillator.

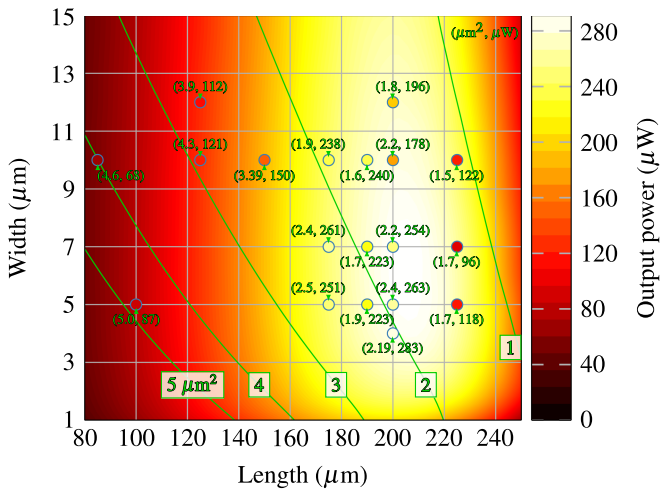

Fig. 7. Color map of the output power of slot-antenna RTD oscillators at 185 GHz. The color-dots represent the experimental data for RTD oscillators working in the frequency range 185 $\pm$ 10 GHz. See other notations in Fig. 6.

As a next step, we include the RTD parasitics in the analysis. We assume the RTD contact resistance of $\rho_c = 2\ \Omega\,\mu\text{m}^2$. The simulation results in this case for the output power at 375 GHz are shown in Fig. 6. The maximum output power does decrease due to the RTD contact resistance; it is $\approx$90 μW now. However, an optimal slot geometry to achieve the global power maximum remains almost the same as in Fig. 5: slot length is $\approx$80–90 μm and the slot width is $\approx$5 μm. Fig. 7 shows similar simulation data for approximately twice lower frequency of 185 GHz. The global maximum of $\approx$300 μW should be achieved for the slot length of $\approx$200–210 μm and the slot width of $\approx$5–6 μm.

Figs. 6 and 7 also include contour lines for the RTD-mesa area required for each combination of the slot length and width to make the oscillator work at the chosen frequencies. The contour lines indicate that the RTD-mesa areas decrease with the increase of w, since the absolute value of the antenna susceptance B_a drops and that needs to be compensated by the reduction of the RTD-mesa area, according to (7). This behavior also aligns with the observation made in [27] that the oscillation frequency increases with the decrease of the slot width. Indeed, one can see the increase of RTD-mesa area with the decrease of w as a means to reduce the oscillation frequency: if the RTD-mesa area would be kept fixed with the decrease of w, then the oscillation frequency would increase. However, decreasing the slot width is not an optimal design strategy: as Figs. 6 and 7 show, if the slot width is made too narrow, then the output power will reduce; there is an optimal parameter range for the slot antennas to get the highest output power at a given frequency. Specifically, for our RTD wafer and for the given frequencies, an optimal slot width is in the range of $\approx$4–8 μm. If the slot width were reduced to 2 μm that should have led to a certain output-power reduction.

V. Sample Fabrication and Measurements

To verify the simulation predictions, we fabricated several batches of samples with different slot-antenna and RTD-mesa dimensions. The oscillator parameters in one batch were chosen to make them operate at 375 GHz. In the second batch, we chose 185 GHz as the target frequency. In the third batch for output power analysis, we fixed the slot width at 4 μm and varied the slot length and RTD-mesa area, resulting in RTD oscillators working at different frequencies. The fabrication process of all these samples was identical.

The fabrication process is based on optical lithography, except for one step. The process started with the deposition of the upper RTD-mesa electrodes: 20/20/160 nm Ti/Pd/Au. The electrodes were then used as a mask and whole areas around RTDs were wet etched $\approx$180 nm down to the n++ bottom layer, forming the RTD mesas. Then, the lower RTD-electrode metallization (20/20/60 nm Ti/Pd/Au) was deposited covering the RTD, but with an opened window for the slot antenna (see schematics in Figs. 1 and 3). The offset of the RTD from the edge of the slot antenna is 3 μm in all our samples. The n++ layers in the slot and the isolation trenches surrounding the lower electrode were later removed by dry etching. As a next step, a 200 nm Si_3N_4 layer was deposited on the entire sample surface. It serves as a passivation layer and as a dielectric in the MIM capacitor (see Fig. 1). As a next step, the Si_3N_4 layer was opened at the tops of the RTD mesas using E-beam lithography. After, a photoresist layer was deposited in the slot-antenna trench next to the RTD as a support layer for the air bridge and then the last metallization layer was deposited (20/280 nm Ti/Au), forming the air bridge across the slot to the RTD and the upper metallization of the MIM capacitor, see an SEM image of a fabricated sample in Fig. 8. As a final step, an ITO shunt resistor was deposited.

The emission spectra of RTD oscillators were measured with a Martin–Puplett interferometer, which has a frequency resolution of $\approx$1 GHz and continues frequency coverage from $\approx$50 GHz to $\approx$5 THz. A Golay cell has been used as a THz detector in the interferometer. Typical measured spectra of several oscillators are shown in Fig. 9. All spectra are clean and do not show any

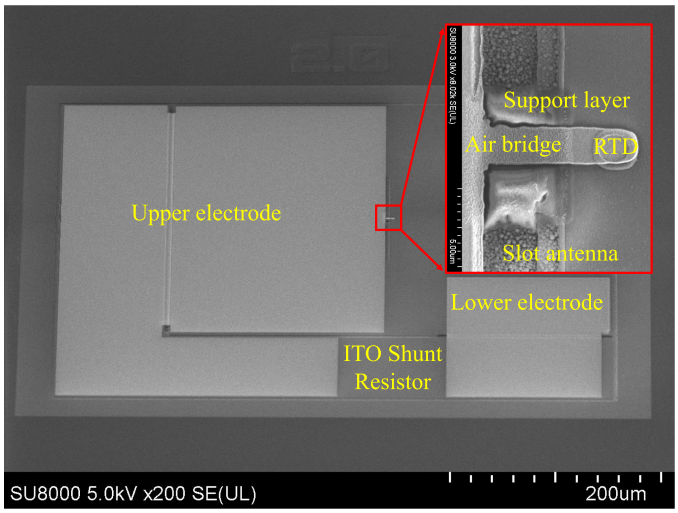

Fig. 8. SEM image of a slot-antenna RTD oscillator with a slot length of 200 μm and width of 4 μm, the RTD mesa was 2.2 μm^2.

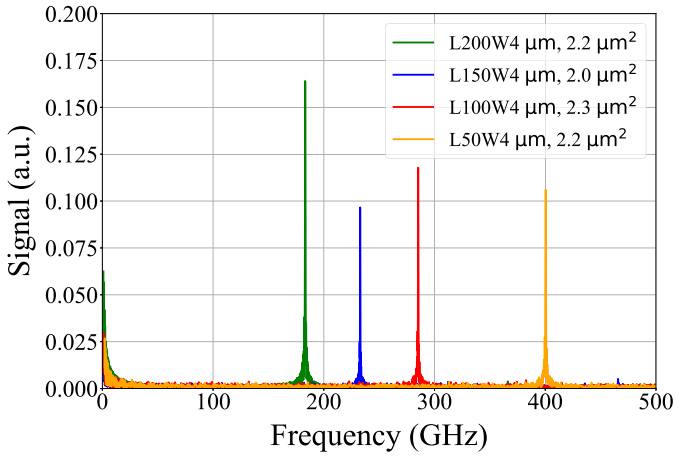

Fig. 9. Measured frequency spectra for oscillators with antenna lengths between 50 and 200 μm, the slot width is 4 μm, and the RTD mesas for these devices were in the range 2.0–2.3 μm^2.

parasitic lower frequency lines, proving that the oscillators were working at the fundamental frequency.

For the output power measurements, as well as during the spectrum measurements above, the oscillator chips were placed on top of a hemispherical Si lens. During the output-power measurements, a calibrated pyroelectric detector was placed directly underneath the Si lens. On the way from the oscillator to the detector, 30 % of the radiation is back-reflected at the Si/air interface and further only a fraction of the radiation in the air is collected by the detector. This fraction is determined by the overlap of the slot-antenna radiation pattern and the input aperture of the detector. Our estimates based on the simulations of the antenna radiation pattern show that only $\approx$ 25 % of the total antenna radiation reaches the detector. Therefore, the emitted oscillator power throughout this article corresponds to the measured detector power multiplied by a factor of 4.

VI. Experimental Data on Symmetrical Slot-Antenna RTD Oscillators

In the first batch of samples, the RTD oscillators were working at the frequencies 375 $\pm$ 10 GHz. The slot antennas had a length in the range of 30–90 μm and a width in the range of 3–8 μm. The RTD-mesa area was adjusted accordingly to match the target frequency of 375 GHz. The measurement and simulation data for the output power of the oscillators are shown in Fig. 6. An oscillation frequency of 368 GHz with an output power of 82 μW was measured for a slot-antenna length and width of 90 μm and 4 μm, respectively, and an RTD area of 0.82 μm^2.

Fig. 7 shows similar measurement and simulation data for the second batch of samples at 185 $\pm$ 10 GHz. The length of the slot antennas was in the range 85–225 μm and the width in the range 4–12 μm. Maximum power of 283 μW was obtained at a frequency of 184 GHz with an antenna length and width of 200 μm and 4 μm, respectively, and an RTD area of 2.2 μm^2.

Several experimental points in Fig. 6 are close to the theoretically expected global maximum of the output power (slot length of $\approx$ 80–90 μm and the slot width of $\approx$ 4–6 μm). The measured output power is the highest at these points. The other experimental points are either outside the global-maximum region or close to its edge; the output power is lower at these points. A similar picture can be seen in Fig. 7. The points for the slot length of $\approx$ 170–200 μm and the slot width of $\approx$ 4–7 μm are close to the global maximum, and the output power is the highest for those samples. The other samples have slot dimensions closer to the edge of the global maximum and the output power is somewhat lower for those samples. However, the experimental data indicate that their maximum is shifted to slightly shorter slots compared to numerical-simulation data. Overall, the experimental data are in reasonably good agreement with the theoretical predictions. We attribute the deviations and certain scattering of the experimental data to the uncontrollable variations of the fabricated samples due to the limitations of the optical lithography used in this study.

The foregoing analysis indicates that an optimum slot-antenna width in the 150–400 GHz frequency range is close to 4 μm. Therefore, as a next step, we fabricated a third batch of RTD oscillators with a slot width of 4 μm and slot lengths of 50 μm, 100 μm, 150 μm, and 200 μm with different RTD-mesa areas, chosen to be close to optima for the highest output power. The output power of these samples is shown in Fig. 10. For each given antenna length, when the RTD area is small, the oscillation frequency is the highest, but the output power is not at the maximum since the RTD current is small. When the RTD area is large, then the frequency is the lowest; still, the output power is getting low again since the radiation conductance of the slot antenna is getting low when the slot antenna is operated much below its eigenfrequency. In between, for some middle values of the RTD area, the oscillator's output power reaches a maximum at certain intermediate frequencies. The experimental data and the theoretical output-power curves in Fig. 10 follow this qualitative behavior. The figure includes additionally several data points corresponding to the samples with the highest output

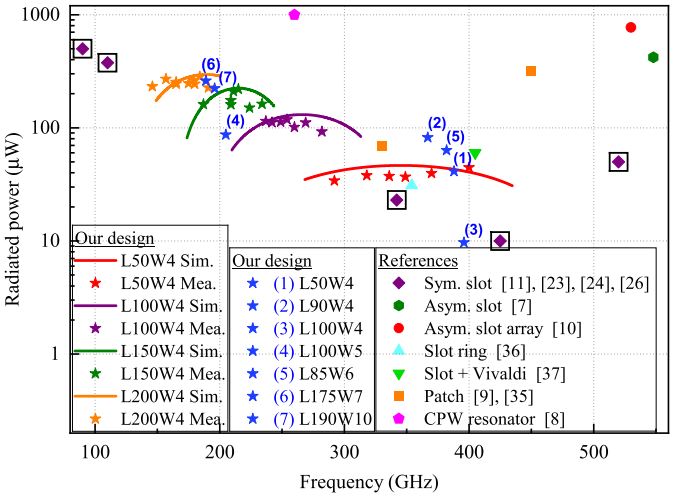

Fig. 10. Radiated power versus oscillation frequency of the fabricated slot antenna RTD oscillators. In this device batch, the slot antenna length was set to 50 μm, 100 μm, 150 μm, and 200 μm, with a constant width of 4 μm. The RTD areas ranged from 2.0 μm^2 to 5.0 μm^2. The solid lines show simulated output power, and the star points indicate the measured ones. In addition, several data points with a high level of output power from the other two batches of samples (see Figs. 6 and 7) are also shown. For comparison, we show the literature data on symmetrical-slot-antenna RTD oscillators and a few characteristic data points for the other types of RTD oscillators.

TABLE I
OUTPUT POWER FOR DIFFERENT TYPES OF RTD OSCILLATORS

References	Frequency GHz	Power μW	Oscillator type
This work	184	283	Sym. slot
	368	82	Sym. slot
[11]	90	500	Sym. slot
[11]	110	376	Sym. slot
[23]	342	23	Sym. slot
[24]	425	10	Sym. slot
[26]	520	50	Sym. slot
[25]	1250	30	Sym. slot
[8]	260	1000	CPW resonator
[35]	330	70	Patch
[36]	354	31	Slot ring
[37]	405	60	Slot + Vivaldi
[9]	450	320	Patch
[7]	548	420	Asym. slot
[20]	660	27	Patch
[38]	730	131	Cavity resonator
[21]	1040	36	Slot + Yagi-Uda
[20]	1090	9	Patch
[9]	450	11800	Patch array
[10]	530	770	Asym.-slot array
[7]	620	610	Asym.-slot array
[10]	630	87	Sym.-slot array
[39]	675	47	CPW array + dipole
[10]	700	300	Asym.-slot array

power from the first two batches of devices with frequencies near 185 GHz and 375 GHz.

The output power of our RTD oscillators in Fig. 10 is very close to the best symmetrical-slot-antenna RTD oscillators reported in the literature. A set of representative literature data for the symmetrical-slot-antenna RTD oscillators is shown in Fig. 10 and in Table I. High output power in our oscillators was achieved due to two reasons. First, the slot-antenna parameters are close to the optimum in our oscillators. Second, due to a small value of τ_{RTD} in our RTDs, which allows one to reduce γ [see (8)], and since our RTDs have a sufficiently large value of the nonlinearity parameter $\alpha(\gamma)$ at small γ. As a result, that leads to large values of the output power, given by (5).

We should stress, that this study is limited to symmetrical-slot-antenna RTD oscillators: RTD oscillators with asymmetrical slot antennas [7] and other types of RTD oscillators do provide even higher output powers. For comparison, Table I shows representative literature data for diverse RTD oscillators: with coplanar-waveguide (CPW) resonators, patch and slot-ring antennas, additional radiators (e.g., Vivaldi or Yagi–Uda antennas), coherent arrays, etc. Different RTD-oscillator types have their advantages and disadvantages, but symmetrical-slot-antenna RTD oscillators stand out due to their simplicity and symmetrical radiation pattern. As such, they still keep their niche in the ongoing investigation and development of RTD oscillators, particularly as a building block in the more complicated and array designs of RTD oscillators [10], [22].

VII. CONCLUSION

In this article, we show that the output power of symmetrical-slot-antenna RTD oscillators depends on the slot width and that the slot width is an important degree of freedom for fine tuning the slot geometry in the RTD oscillators. Our data also indicate that the commonly used 4 μm slot width is close to an optimal slot-parameter range, corresponding to the global output-power maximum, at least in the sub-THz frequency range. This is confirmed both by our theoretical and experimental data.

In the framework of a simplified slot-antenna RTD-oscillator model, we show that there is a universal (independent of the RTD properties) optimal slot width for each slot length. This optimal width is frequency and, in general, slot-material dependent. The existence of such an optimal width is related to an intricate balance between the slot radiation and ohmic losses and slot susceptance resulting in a maximum of the RTD oscillation amplitude. The global output-power maximum of an RTD oscillator is further achieved by a proper choice of slot length, which is already RTD-specific. The optimal slot-geometry predictions of the simplified model are quite close to a global optimum according to an accurate oscillator analysis. This simplified model is useful for semiquantitative or at least qualitative analysis of RTD oscillators.

We also present an extensive set of experimental data on RTD oscillators with different slot widths. The data reasonably agree with the theoretical analysis and support its validity. Some oscillators exhibit an output-power level close to the state-of-the-art for fundamental-frequency symmetrical-slot-antenna RTD oscillators in the frequency range of 150–400 GHz. Specifically, we report 283 μW at 184 GHz and 82 μW at 368 GHz.

ACKNOWLEDGMENT

The authors would like to thank the Center for Micro- and Nanostructures for providing clean-room facilities.

REFERENCES

[1] K. Sengupta, T. Nagatsuma, and D. M. Mittleman, "Terahertz integrated electronic and hybrid electronic–photonic systems," *Nature Electron.*, vol. 1, no. 12, pp. 622–635, 2018.

[2] M. Asada and S. Suzuki, "Room-temperature oscillation of resonant tunneling diodes close to 2 THz and their functions for various applications," *J. Infrared Millimetre Terahertz Waves*, vol. 37, pp. 1185–1198, 2016.

[3] M. Feiginov, "Frequency limitations of resonant-tunnelling diodes in sub-THz and THz oscillators and detectors," *J. Infrared Millimetre Terahertz Waves*, vol. 40, pp. 365–394, 2019.

[4] M. Feiginov, C. Sydlo, O. Cojocari, and P. Meissner, "Resonant-tunnelling-diode oscillators operating at frequencies above 1.1 THz," *Appl. Phys. Lett.*, vol. 99, 2011, Art. no. 233506.

[5] R. Izumi, S. Suzuki, and M. Asada, "1.98 THz resonant-tunneling-diode oscillator with reduced conduction loss by thick antenna electrode," in *Proc. 42nd Int. Conf. Infrared, Millimeter, Terahertz Waves*, 2017, pp. 1–2.

[6] D. T. Nguyen, P. Ourednik, and M. Feiginov, "Island THz on-chip slot-antenna resonant-tunneling-diode oscillators," *Appl. Phys. Lett.*, vol. 123, no. 4, 2023, Art. no. 043508.

[7] S. Suzuki, M. Shiraishi, H. Shibayama, and M. Asada, "High-power operation of terahertz oscillators with resonant tunneling diodes using impedance-matched antennas and array configuration," *IEEE J. Sel. Top. Quantum Electron.*, vol. 19, no. 1, Jan./Feb. 2013, Art. no. 8500108.

[8] A. Al-Khalidi et al., "Resonant tunneling diode Terahertz sources with up to 1 mW output power in the J-band," *IEEE Trans. THz Sci. Technol.*, vol. 10, no. 2, pp. 150–157, Mar. 2020.

[9] Y. Koyama et al., "A high-power terahertz source over 10 mW at 0.45 THz using an active antenna array with integrated patch antennas and resonant-tunneling diodes," *IEEE Trans. THz Sci. Technol.*, vol. 12, no. 5, pp. 510–519, Sep. 2022.

[10] T. V. Mai, M. Asada, T. Namba, Y. Suzuki, and S. Suzuki, "Coherent power combination in a resonant-tunneling-diode arrayed oscillator with simplified structure," *IEEE Trans. THz Sci. Technol.*, vol. 13, no. 4, pp. 405–414, Jul. 2023.

[11] C. Spudat, P. Ourednik, G. Picco, D. T. Nguyen, and M. Feiginov, "Limitations of output power and efficiency of simple resonant-tunneling-diode oscillators," *IEEE Trans. THz Sci. Technol.*, vol. 13, no. 1, pp. 82–92, Jan. 2023.

[12] N. Oshima, K. Hashimoto, S. Suzuki, and M. Asada, "Terahertz wireless data transmission with frequency and polarization division multiplexing using resonant-tunneling-diode oscillators," *IEEE Trans. THz Sci. Technol.*, vol. 7, no. 5, pp. 593–598, Sep. 2017.

[13] J. Webber et al., "Multi-level wireless transmission using resonant tunneling diodes in 300-GHz band," *Electron. Lett.*, vol. 59, no. 5, 2023, Art. no. e12731.

[14] T. Miyamoto, A. Yamaguchi, and T. Mukai, "Terahertz imaging system with resonant tunneling diodes," *Japanese J. Appl. Phys.*, vol. 55, 2016, Art. no. 032201.

[15] K. Okamoto et al., "Terahertz sensor using photonic crystal cavity and resonant tunneling diodes," *J. Infrared Millimeter Terahertz Waves*, vol. 38, pp. 1085–1097, 2017.

[16] A. Dobroiu, R. Wakasugi, Y. Shirakawa, S. Suzuki, and M. Asada, "Absolute and precise terahertz-wave radar based on an amplitude-modulated resonant-tunneling-diode oscillator," *Photonics*, vol. 5, no. 4, 2018, Art. no. 52.

[17] P. Ourednik and M. Feiginov, "Chip-size double-resonant-tunneling-diode patch-antenna oscillators and their sub-THz application," in *Proc. 15th U.K.-Europe-China Workshop Millimetre-Waves Terahertz Technol.*, 2022, pp. 1–3.

[18] S. Makhlouf et al., "Terahertz sources and receivers: From the past to the future," *IEEE J. Microw.*, vol. 3, no. 3, pp. 894–912, Jul. 2023.

[19] E. R. Brown et al., "Oscillations up to 712 GHz in InAs/AlSb resonant-tunneling diodes," *Appl. Phys. Lett.*, vol. 58, pp. 2291–2293, 1991.

[20] P. Ourednik and M. Feiginov, "Double-resonant-tunneling-diode bridgeless patch-antenna oscillators operating up to 1.09 THz," *Appl. Phys. Lett.*, vol. 120, no. 18, 2022, Art. no. 183501.

[21] K. Kasagi, S. Suzuki, and M. Asada, "Large-scale array of resonant-tunneling-diode terahertz oscillators for high output power at 1 THz," *J. Appl. Phys.*, vol. 125, no. 15, 2019, Art. no. 151601.

[22] D. J. Headland, Y. Nishida, X. Yu, M. Fujita, and T. Nagatsuma, "Terahertz oscillator chips backside-coupled to unclad microphotonics," *IEEE J. Sel. Top. Quantum Electron.*, vol. 29, no. 3, May/Jun. 2023, Art. no. 8500111.

[23] N. Orihashi, S. Hattori, S. Suzuki, and M. Asada, "Experimental and theoretical characteristics of sub-terahertz and terahertz oscillations of resonant tunneling diodes integrated with slot antennas," *Japanese J. Appl. Phys.*, vol. 44, no. 11R, 2005, Art. no. 7809.

[24] N. Kishimoto, S. Suzuki, A. Teranishi, and M. Asada, "Frequency increase of resonant tunneling diode oscillators in Sub-THz and THz range using thick spacer layers," *Appl. Phys. Exp.*, vol. 1, no. 4, 2008, Art. no. 042003.

[25] H. Kanaya, R. Sogabe, T. Maekawa, S. Suzuki, and M. Asada, "Fundamental oscillation up to 1.42 THz in resonant tunneling diodes by optimized collector spacer thickness," *J. Infrared Millimetre Terahertz Waves*, vol. 35, pp. 425–431, 2014.

[26] M. Feiginov, H. Kanaya, S. Suzuki, and M. Asada, "Operation of resonant-tunneling diodes with strong back injection from the collector at frequencies up to 1.46 THz," *Appl. Phys. Lett.*, vol. 104, 2014, Art. no. 243509.

[27] S. Suzuki, N. Kishimoto, M. Asada, N. Sekine, and I. Hosako, "Experimental and theoretical investigation of the dependence of oscillation characteristics on structure of integrated slot antennas in sub-terahertz and terahertz oscillating resonant tunneling diodes," *Japanese J. Appl. Phys.*, vol. 47, no. 1R, 2008, Art. no. 64.

[28] H. Shibayama, M. Shiraishi, S. Suzuki, and M. Asada, "High-power operation of terahertz oscillators with resonant tunneling diodes using offset-fed slot antennas and array configuration," *J. Infrared Millimeter Terahertz Waves*, vol. 33, pp. 475–478, 2012.

[29] M. Feiginov, "Effect of the coulomb interaction on the response time and impedance of the resonant-tunneling diodes," *Appl. Phys. Lett.*, vol. 76, pp. 2904–2906, 2000.

[30] M. Feiginov, "Does the quasibound-state lifetime restrict the high-frequency operation of resonant-tunnelling diodes?," *Nanotechnol.*, vol. 11, 2000, Art. no. 359.

[31] M. Feiginov, "Displacement currents and the real part of high-frequency conductance of the resonant-tunneling diode," *Appl. Phys. Lett.*, vol. 78, pp. 3301–3303, 2001.

[32] M. Feiginov and D. R. Chowdhury, "Operation of resonant-tunneling diodes beyond resonant-state-lifetime limit," *Appl. Phys. Lett.*, vol. 91, 2007, Art. no. 203501.

[33] P. Ourednik, G. Picco, D. T. Nguyen, C. Spudat, and M. Feiginov, "Large-signal dynamics of resonant-tunneling diodes," *J. Appl. Phys.*, vol. 133, no. 1, 2023, Art. no. 014501.

[34] C. A. Balanis, *Antenna Theory*, 4th ed. Hoboken, NJ, USA: Wiley, 2015.

[35] P. Ourednik, T. Hackl, C. Spudat, D. T. Nguyen, and M. Feiginov, "Double-resonant-tunneling-diode patch-antenna oscillators," *Appl. Phys. Lett.*, vol. 119, no. 26, 2021, Art. no. 263509.

[36] S. Iwamatsu, Y. Nishida, M. Fujita, and T. Nagatsuma, "Terahertz coherent oscillator integrated with slot-ring antenna using two resonant tunneling diodes," *Appl. Phys. Exp.*, vol. 14, no. 3, 2021, Art. no. 034001.

[37] K. Urayama et al., "Sub-terahertz resonant tunneling diode oscillators integrated with tapered slot antennas for horizontal radiation," *Appl. Phys. Exp.*, vol. 2, no. 4, 2009, Art. no. 044501.

[38] F. Han, H. Fujikata, H. Tanaka, S. Suzuki, and M. Asada, "Terahertz oscillator using rectangular-cavity resonator and large-area RTD with heat dissipation structure," in *Proc. 47th Int. Conf. Infrared, Millimeter, Terahertz Waves*, 2022, pp. 1–2.

[39] M. Kim, J. Lee, J. Lee, and K. Yang, "A 675 GHz differential oscillator based on a resonant tunneling diode," *IEEE Trans. THz Sci. Technol.*, vol. 6, no. 3, pp. 510–512, May 2016.

Dinh Tuan Nguyen received the B.E. and M.E. degrees in electrical engineering from the Moscow Institute of Physics and Technology, Moscow, Russia, in 2010 and 2012, respectively. He has been working toward the Ph.D. degree in electrical engineering with the Technische Universität Wien, Vienna, Austria, since 2018.

From 2013 to 2019, he was with Le Quy Don Technical University, Hanoi, Vietnam, as a Teaching Assistant and Lecturer. His research interests include THz electronics.

Gabriele Picco received the B.Sc. and M.Sc. degrees in physics from the Universitá degli studi di Trieste, Trieste, Italy, in 2016 and 2019, respectively. Since 2021, he has been working toward the Ph.D. degree in electrical engineering with Technische Universität Wien, Vienna, Austria.

His research interests include semiconductor physics and THz electronics.

Petr Ourednik received the B.E. and M.E. degrees in electrical engineering from Czech Technical University, Prague, Czech Republic, in 2014 and 2016, respectively, and the Ph.D. degree in electrical engineering from the Technische Universität Wien, Vienna, Austria, in 2023.

From 2016 to 2018, he was with the Czech Technical University, as a Research Associate. Since 2018, he has been with the Technische Universität. His research interests include high-frequency and THz electronics.

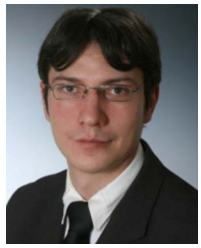

Christian Spudat received the M.Sc. degree in physics from Freie Universität Berlin, Berlin, Germany, in 2006 and the Ph.D. degree in physics from the Universität Duisburg-Essen, Duisburg, Germany, in 2010.

From 2006 to 2010, he was with the Research Center Jülich, Jülich, Germany, as a Research Associate. From 2011 to 2015, he was with the Fraunhofer Institute for Electronic Nano Systems, Chemnitz, Germany, as a Researcher. Since 2016, he has been with the Technische Universität Wien, Vienna, Austria, as a Researcher. His research interests include carbon nanostructures and THz electronics.

Michael Feiginov received the M.Sc. degree in electrical engineering and physics from the Moscow Institute of Physics and Technology, Moscow, Russia, in 1994, and the Ph.D. degree in physics of semiconductors and dielectrics from the Institute of Radioengineering and Electronics, Russian Academy of Sciences, Moscow, in 1999.

From 1994 to 2000, he was with the Institute of Radioengineering and Electronics, Russian Academy of Sciences, as a Junior Scientist, Scientist, and Senior Scientist. In 2001, he was with the Technische Universität Chemnitz, Chemnitz, Germany, as a Researcher. From 2002 to 2013, he was with the Technische Universität Darmstadt, Darmstadt, Germany, as a Senior Researcher. From 2013 to 2014, he was with the Tokyo Institute of Technology, Tokyo, Japan as a Visiting Researcher. From 2014 to 2016, he was with Canon Inc., Tokyo, as a Scientific Manager with Frontier Research Center. Since 2016, he has been a Professor with Technische Universität Wien, Vienna, Austria. His research interests include THz electronics and photonics.